View metadata, citation and similar papers at core.ac.uk

brought to you by CORE

provided by Elsevier - Publisher Connector

Current Biology 18, 1365–1372, September 23, 2008 ©2008 Elsevier Ltd All rights reserved DOI 10.1016/j.cub.2008.07.095

Article

Transducer-Based Force Generation Explains Active Process in *Drosophila* Hearing

Björn Nadrowski,[1,*] Jörg T. Albert,[1,2] and Martin C. Göpfert[1,*]
[1]Sensory Systems Lab
Institute of Zoology
University of Cologne
Weyertal 119
50923 Cologne
Germany

Summary

Background: Like vertebrate hair cells, *Drosophila* auditory neurons are endowed with an active, force-generating process that boosts the macroscopic performance of the ear. The underlying force generator may be the molecular apparatus for auditory transduction, which, in the fly as in vertebrates, seems to consist of force-gated channels that occur in series with adaptation motors and gating springs. This molecular arrangement explains the active properties of the sensory hair bundles of inner-ear hair cells, but whether it suffices to explain the active macroscopic performance of auditory systems is unclear.
Results: To relate transducer dynamics and auditory-system behavior, we have devised a simple model of the *Drosophila* hearing organ that consists only of transduction modules and a harmonic oscillator that represents the sound receiver. In vivo measurements show that this model explains the ear's active performance, quantitatively capturing displacement responses of the fly's antennal sound receiver to force steps, this receiver's free fluctuations, its response to sinusoidal stimuli, nonlinearity, and activity and cycle-by-cycle amplification, and properties of electrical compound responses in the afferent nerve.
Conclusions: Our findings show that the interplay between transduction channels and adaptation motors accounts for the entire macroscopic phenomenology of the active process in the *Drosophila* auditory system, extending transducer-based amplification from hair cells to fly ears and demonstrating that forces generated by transduction modules can suffice to explain active processes in ears.

Introduction

Ears are prime examples of complex dynamical systems. They consist of a multitude of interacting macroscopic, cellular, and molecular components. They are nonlinear, operate away from thermal equilibrium, and rely on positive mechanical feedback to improve their sensitivity to sound [1–7]: Inside the ear, sound-induced vibrations are coupled to mechanosensory cells and molecules that transduce these vibrations into electrical signals and, in addition, generate forces to augment the vibrations they transduce [2–8]. This mechanical feedback, which in vertebrates is known as the "cochlear amplifier" [9, 10], accounts for vital characteristics in auditory-system performance. These characteristics include (1) a compressive nonlinearity that makes the ear more sensitive as the sound intensity declines, (2) an increased frequency selectivity due to frequency-specific cycle-by-cycle amplification, (3) power gain, reflecting active energy contributions, and (4) self-sustained feedback oscillations that arise from excess amplification and can cause ringing in the ear [2–11].

Signatures of mechanical-feedback amplification have been documented for vertebrate and invertebrate auditory systems [3–5, 7, 8, 11–13], yet linking the macroscopic phenomenology of this amplification to molecular processes has proven difficult because of the complicated functional anatomy and limited experimental accessibility of most animals' ears [4, 11, 14]. In vertebrates, all the four key characteristics of the cochlear amplifier have been observed in the hair-bundle mechanics of inner-ear hair cells [15–18]; such observations allow us to relate these physical properties to molecular processes on the level of cells. A theoretical framework that relates hair-bundle mechanics and molecular processes is the gating-spring model of mechanosensory transduction [19–22]. This model explains mechanical correlates of transducer gating and adaptation betrayed by the hair bundle's response to force steps by assuming that hair-bundle deflections directly gate transducer channels that are arranged in series with adaptation motors and gating springs. When supplemented with feedback between channels and motors, this molecular arrangement explains active hair-bundle mechanics [23–25], supporting the molecular modules for transduction as candidate force generators for active amplification in ears [26].

Much as sensory hair bundles have been used to test the relation between transduction and amplification in inner-ear hair cells, the antennal sound receiver of *Drosophila melanogaster* can be used to test this relation for a whole ear: First, because it sticks out from the body, the fly's sound receiver is freely accessible to mechanical examination, allowing us to probe auditory performance in vivo without compromising the integrity of the ear [27]. Second, like a hair bundle, this antennal receiver displays key characteristics of the cochlear amplifier, for which the source of activity has been traced down to the mechanosensory neurons that connect to the receiver's base [28–30]. Third, the fly's antennal receiver also displays hair-bundle-like correlates of transducer gating and adaptation [31], raising the possibility that a transduction mechanism like that proposed for vertebrate hair cells promotes amplification in the fly's antennal ear. To test this hypothesis, we devised a simple gating-spring model of the *Drosophila* hearing organ that incorporates feedback between channels and motors and takes the ear's basic anatomy into account. We then systematically explored the active in vivo performance of the fly's auditory system by measuring displacement responses of the antennal sound receiver under different stimulus conditions and by recording mechanically evoked compound responses from the afferent nerve. Comparison between measured and simulated data shows that the model quantitatively explains the ear's macroscopic performance, linking the active behavior of an intact auditory system to transduction events.

*Correspondence: bjoern.nadrowski@uni-koeln.de (B.N.), m.gopfert@uni-koeln.de (M.C.G.)
[2]Present address: UCL Ear Institute, University College London, 332 Gray's Inn Road, London WC1X 8EE, UK

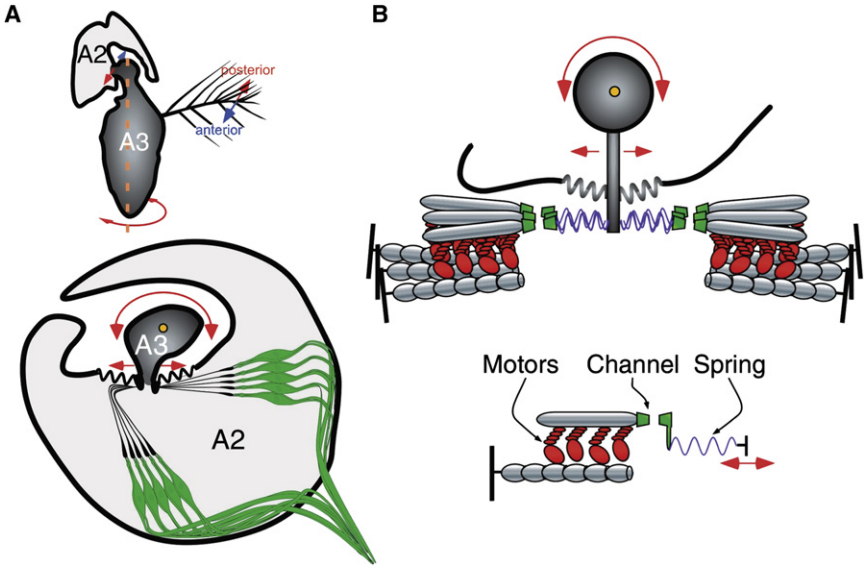

Figure 1. Transducer-Based Model of the *Drosophila* Ear

(A) Auditory anatomy. Top: front view of the antenna depicting the two distal antennal segments (A2 and A3) and the feathery arista. Bottom: cross-section through the joint between A2 and A3. The arista and A3 constitute the sound receiver. A2 houses two opposed populations of mechanosensory neurons that perpendicularly connect to the receiver. Arrows indicate the direction of stimulus-evoked receiver movements.
(B) Schematic model consisting of two opposing populations of transducer modules that symmetrically couple to a common harmonic oscillator. Each transducer module is formed by one ion channel, a set of adaptation motors, and one gating spring. Please note that the myosin-like appearance of the motors has been chosen merely for iconographic reasons and must not be misunderstood as a speculation about the molecular identities of the motors.

Results

Transducer-Based Model of the *Drosophila* Hearing Organ

In *Drosophila*, the third segment of the antenna and its lateral arista serve as a sound receiver (Figure 1A): When stimulated acoustically, this segment and its arista sympathetically twist back and forth as a rigid body about an antennal joint [27, 32]. Vibrations of the receiver are directly coupled to—and transduced by—Johnston's organ, a chordotonal stretch-receptor organ in the antenna's second segment [32–34]. This organ houses two opposed populations of mechanosensory neurons that, spanning across the joint, perpendicularly connect to the receiver's anterior and posterior sides [32–34] (Figure 1A).

Consistent with previous observations [29, 31], we describe this auditory system as two opposed transducer populations that couple to a simple harmonic oscillator that represents the antennal sound receiver (Figure 1B). The spring constant of the harmonic oscillator accounts for the linear elastic properties of Johnston's organ and the antennal joint. Both transducer populations are assumed to house equal numbers of parallel transducer modules, with each module conforming to the gating-spring model in that it consists of one ion channel, a set of adaptation motors, and one gating spring (Figure 1B). For simplicity, we suppose that the motors are characterized by a linear force-velocity relation and that each channel is either open or closed. The open probability of the channels is given by a sigmoid function of the gating-spring tension [21, 22] (Supplemental Data available online). This sigmoid function constitutes the only nonlinearity in our model. Feedback between channels and motors is implemented by linearly coupling the force-velocity characteristic of the motors to the open probability of the associated channels [23–25]. The dynamic properties of the model, which is explicitly mirror symmetric with respect to the direction of forcing, are described by four coupled first-order differential equations with nine free parameters, three of which refer to the harmonic oscillator representing the fly's antennal sound receiver (Supplemental Data).

To explore whether this simple model explains auditory-system performance, we sequentially monitored the displacement of a fly's antennal receiver under various stimulus conditions. On the basis of this experimental data, model parameters were adjusted for each fly by performing two types of fits (Supplemental Data). For one, the model was fitted to the receiver's response to an individual force step of given polarity and amplitude, which we refer to as an "individual fit"; for the other, the model was simultaneously fitted (1) to the receiver's responses to ten small force steps of different polarity and amplitude, (2) to the receiver's linear response function obtained for weak sinusoidal forcing, and (3) to the spectral density of its free fluctuations in the absence of forcing. The resulting fit, which was run for each of the seven receivers examined, is referred to as the "general fit" (for parameter values, see Table S1). Figures 2–4 and Figure S1 show measurements and fits for one representative receiver; the respective general and individual fits shown in these figures were computed with the parameter values provided for fly 6 in Table S1. General-fit parameters obtained for other receivers are also provided in Table S1.

Receiver Response to Force Steps Betrays Temporal Evolution of Transduction Events

To test for mechanical correlates of transducer gating and adaptation, we first exposed the fly's antennal sound receiver to force steps and measured its displacement response. In accord with previous observations [31], this response displayed a characteristic pattern, including an initial overshoot in the forcing direction that was followed by a rebound and a damped oscillation before a constant steady-state position was reached (Figure 2A). Whereas the latter steady-state position scaled linearly with the amplitude of forcing, the height of the initial overshoot displayed a nonlinear force dependence, with the corresponding dynamic stiffness being minimal at approximately zero forcing (Figure 2A). These force-displacement characteristics were accurately reproduced by the general fit of the model (Figure 2A), which also captured the gross pattern of the receiver's response to individual steps (Figure 2B). Individual fits, in turn, reproduced even fine details of this pattern (Figure 2B, gray lines) while still approximating the general force-displacement characteristics (Figure 2A). As judged from the model, the transient nonlinearity observed upon stimulus onset results from transducer gating (Figure 2C). Because the stationary open probability of the channels is ~0.5 (Table

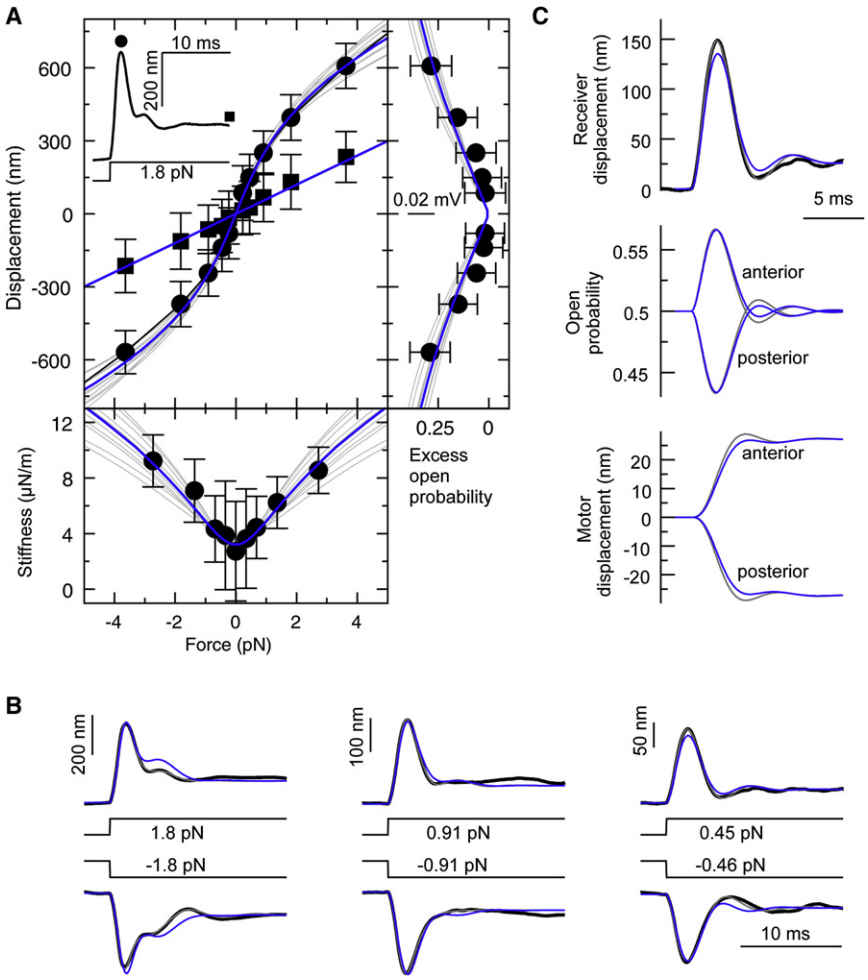

Figure 2. Mechanical Response to Force Steps

(A) Top: temporal pattern of the displacement response of the arista tip to a force step (inset) and force-displacement relations. The relations are shown for the receiver's initial displacement peak (represented by circles) and its steady-state displacement (represented by squares). Lines represent force-displacement relations obtained by numerically integrating the model equations with parameter values of general (blue) and individual (gray) fits. Bottom: corresponding slope stiffness at the initial displacement peak. Right: peak excess channel open probability (Supplemental Data) predicted by general and individual fits and superimposed amplitude of compound action potentials in the antennal nerve (represented by circles); CAP amplitudes are defined as the voltage difference between the positive and negative peaks after the onset of a force step (see Figure 4E, bottom panels). All measured data (symbols) represent the averages of 200–300 repetitions. Errors bars indicate standard deviations.

(B) Time traces of the receiver's displacement response to six force steps of different polarity and amplitude (black) and corresponding general (blue) and individual (gray) fits.

(C) Temporal relation between receiver displacement, channel open probabilities, and motor displacements predicted by general (blue) and individual (gray) fits. Open probabilities and motor displacements are shown for both transducer populations. Motor displacements arising at the molecular level are projected to the receiver; because of the completeness of adaptation, projected motor displacements equal the steady-state displacement of the receiver. All data refer to fly 6 (for parameter values, see Table S1).

S1), the gating of channels of both transducer populations contributes equally to the initial overshoot in the receiver's displacement response: Assuming a geometry as depicted in Figure 1B, forcing the receiver in the anterior (positive) direction opens channels of the anterior transducer population, thereby nonlinearly reducing the tension of the anterior gating springs and facilitating the receiver's movement in the direction of the force. At the same time, the closing of channels of the posterior transducer population nonlinearly increases the tension of the posterior gating springs, a phenomenon that also facilitates the receiver's movement in the direction of the force. The rebound in the receiver's response coincides with movements of the adaptation motors, which restore the open probability of the channels by readjusting the gating-spring tension (Figure 2C). As judged from the model, these motor movements are fast, with time constants between 4 and 12 ms (Table S2). After ~10 ms, the motors have reached their final position, and the stationary open probability of the transducer channels (~0.5) is completely restored (Figure 2C). The damped oscillation, which is seen in both measured and modeled responses (Figure 2B), is explained by inertial effects due to the receiver's mass in combination with elastic components.

Interplay Between Transduction Channels and Adaptation Motors Explains Active Receiver Response to Sinusoidal Forcing

To test for active amplification in the fly's auditory system, we next measured the receiver's displacement response to a multisine force stimulus consisting of 38 sinusoids of equal amplitude. For each stimulus frequency, we determined the respective Fourier transforms of the receiver's displacement and the stimulus force, whereby the response function of the receiver was calculated as the ratio between both (Supplemental Data). For weak forces ($\lesssim$ ~0.1 pN), this response function was independent of the amplitude of forcing, defining the linear response function $\tilde{\chi}_0$ of the system. The real and imaginary parts of this linear response function resembled that of a simple harmonic oscillator for frequencies $\gtrsim$ ~200 Hz (Figure 3A). At lower frequencies, however, a striking difference was observed: The imaginary part changed sign around the receiver's best frequency [BF($|\tilde{\chi}_0|$), i.e., the frequency at which the amplitude of the linear response function is maximal; 183 ± 35 Hz, n = 7], assuming negative values at frequencies considerably below BF($|\tilde{\chi}_0|$) (Figure 3A). The imaginary part of the linear response function is proportional to the energy the stimulus provides to the system. A negative imaginary part signifies activity: Instead of providing energy, the stimulus consumes energy from the system. This active behavior can be visualized by plotting the average phase-locked displacement per stimulus cycle against the stimulus force (Figure 3C). The area enclosed by the circles represents the average work per stimulus cycle, whereby clockwise rotation means that work is provided to the system and counter-clockwise rotation means that the systems actively provides work. The general fit of the model reproduced this active behavior, including the negative imaginary part of the measured linear response

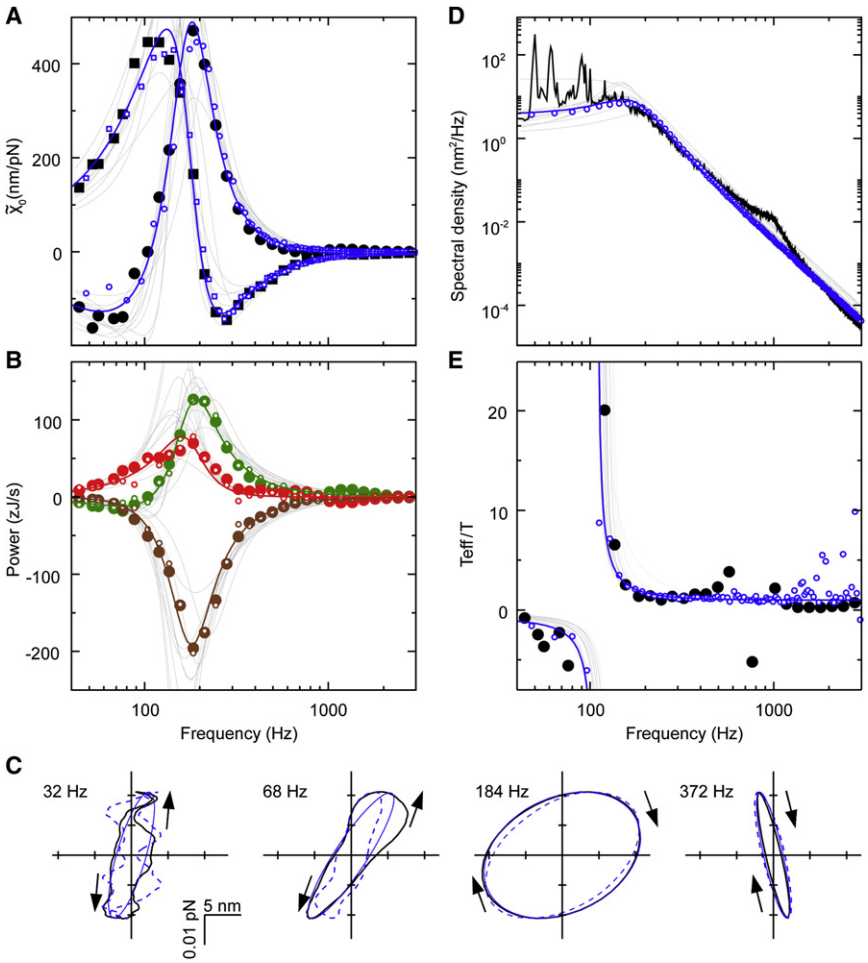

Figure 3. Mechanical Response to Sinusoidal Stimulation and Free Fluctuations

(A) Linear response function of the sound receiver (same receiver as in Figure 1; stimulus force: 0.02 pN). Filled symbols: measured response function (squares indicate the real part, circles the imaginary part). Lines: analytically calculated real and imaginary parts of the linear response function with parameter values of general (blue) and individual (gray) fits. Open symbols indicate stochastic simulations based on the general fit.

(B) Corresponding power characteristics. Green: power provided by the force stimulus; brown: power dissipated by the receiver; red: active power production betrayed by the difference between stimulus power and power dissipation. Filled symbols: experimental data; lines: analytically calculated powers with general (colored) and individual (gray) fit parameters; open symbols: stochastic simulations based on the general fit.

(C) Corresponding average displacement-force cycles for different stimulus frequencies. Black lines: experimental data; straight blue lines: analytical calculations based on general-fit parameters; hatched blue lines: stochastic simulations based on general-fit parameters. Clockwise circulation signals that the receiver takes up energy from the stimulus; counterclockwise circulation signals that the receiver actively provides work.

(D) Power spectrum of the receiver's free fluctuations. Black indicates measured power spectrum. Blue and gray lines and symbols as in (A).

(E) Normalized effective temperature (Supplemental Data). Symbols and colors as in (A). All data are from fly 6 (for parameter values, see Table S1).

function (Figure 3A) and the direction and shape of the force-displacement cycles (Figure 3C). As judged from the model, the activity emerges from shifts of the motors' force-velocity characteristics due to transducer gating: If the force-velocity characteristic of the adaptation motors is kept constant (i.e., if the feedback between channel open probabilities and motor activities is turned off), the imaginary part of the linear response function assumes positive values for all frequencies, and the system becomes entirely passive.

For a passive system, the average power provided by an external stimulus, $\overline{P}_S$, is balanced by dissipation, $\overline{P}_D$, with $\overline{P}_S + \overline{P}_D = 0$. If the system is active, dissipation can exceed the stimulus power, $\overline{P}_S < -\overline{P}_D$, resulting in power gain, $\overline{P}_A$, with $\overline{P}_A = -\overline{P}_D - \overline{P}_S$. On the basis of the general-fit parameters, this power gain can be estimated for the ear of the fly (Figure 3B): $\overline{P}_S$ can be deduced from the external stimulus force F_{ext} and the average vibration velocity $\dot{X}$ of the receiver, $\overline{P}_S = 1/T \int_0^T F_{ext}\dot{X}dt$. $\overline{P}_S$ is negative when the imaginary part of the linear response function is negative, meaning that the fly's antennal receiver actively works against the stimulus force. $\overline{P}_D$, in turn, can be deduced from the friction constant λ of the receiver, $\overline{P}_D = -1/T \int_0^T \lambda \dot{X}^2 dt$, providing a conservative estimate of $\overline{P}_D$ (and $\overline{P}_A$) as internal dissipation is neglected. The power gain, $\overline{P}_A$, peaked at a frequency $F(\overline{P}_A)_{peak}$, close to the best frequency of the receiver [$F(\overline{P}_A)_{peak}$ = 1.03 ± 0.14BF($|\tilde{\chi}_0|$), n = 7] (Figure 3B). At $F(\overline{P}_A)_{peak}$, $\overline{P}_S$ was positive, meaning that the receiver is powered by both the external stimulus and the activity of adaptation motors. $\overline{P}_A$ ranged between 59 and 462 zJ/s (189 ± 158 zJ/s, n = 7) at $F(\overline{P}_A)_{peak}$, corresponding to 0.3 to 0.9 (0.6 ± 0.2, n = 7) times the stimulus power. When internal dissipation due to motor friction was taken into account (Supplemental Data), $\overline{P}_A$ exceeded the stimulus power at all frequencies, yielding $\overline{P}_A$ = 2.34 ± 1.28 $\overline{P}_S$ at $F(\overline{P}_A)_{peak}$.

Fluctuations and Nonequilibrium Thermodynamics

In the absence of external stimuli, the fly's antennal receiver erratically twitches back and forth. To test whether our model describes these free fluctuations, we added simple noise terms to the deterministic model equations [23] (Supplemental Data). The spectral density of the model's free fluctuations was analytically calculated to linear order and used for the general fit. Modeled and measured spectral density curves displayed similar amplitudes and shapes (Figure 3D).

The independent measurements of the receiver's linear response function (Figure 3A) and its free fluctuations (Figure 3D) allow us to quantify deviations from equilibrium thermodynamics: By using the fluctuation-dissipation theorem [16, 23], we can define a frequency-specific effective temperature, T_{eff}, which, for a passive system such as a harmonic oscillator, will equal the ambient temperature T (Supplemental Data). For the antennal receiver, the measurements yielded $T_{eff} \neq T$ for all frequencies (Figure 3E). This behavior was reproduced by the general fit of the model, which predicts that T_{eff}

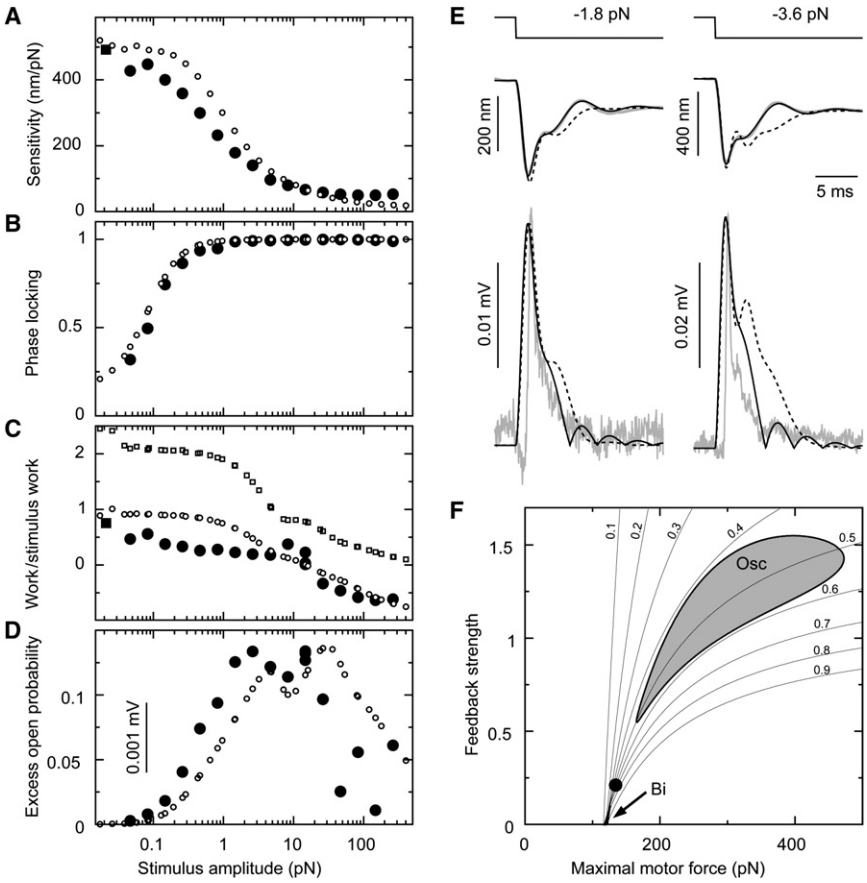

Figure 4. Nonlinearity, State Diagram, and Nerve Response

(A) Mechanical sensitivity of the receiver to sinusoidal forcing at its best frequency (156 Hz, same receiver as in Figures 2 and 3). Filled circles: experimental data obtained for single-sine stimulation; open circles: noisy simulation based on the general fit; filled square: sensitivity obtained for the multisine-stimulus (Figure 2).

(B) Corresponding phase locking of measured and simulated displacement responses by the external stimulus force (Supplemental Data).

(C) Corresponding active work provided by the receiver per stimulus cycle, normalized to the stimulus work. Symbols are as in (A). Open squares correspond to the active contribution of the molecular motors, taking internal friction into account (Supplemental Data).

(D) Corresponding nerve response and excess open probability. Fourier amplitudes were calculated at twice the stimulus frequency to account for the frequency doubling of the nerve response [31]. Filled circles represent Fourier amplitudes of CAP responses; open circles represent Fourier amplitudes of the excess open probability taken from stochastic simulations (Supplemental Data).

(E) Mechanically evoked nerve responses. Gray lines represent measured receiver displacement (middle) and CAP response (bottom) to force steps (top). Black lines represent receiver displacement and excess open probability predicted by individual (straight) and general (hatched) fits. Excess open probabilities are individually scaled to match the peak amplitude of the CAP (Supplemental Data).

(F) State diagram depicting the dynamical states of the system in dependence of the maximal force the adaptation motors develop when the channels are closed and the strength of the feedback that couples the motor force to the open probability of the channels. Other model parameters are fixed to those of the general fit. Osc: oscillatory regime (depicted in gray); Bi: bistable regime. Monostable states are predicted for all the other parameter combinations. Oscillating and monostable regimes are separated by a Hopf bifurcation. Lines of constant open probability are shown as thin black lines. Parameter values of the general fit are marked by the black circle. All data refer to fly 6 (for parameter values, see Table S1).

approaches T only at frequencies >> BF($|\tilde{\chi}_0|$) (Figure 3E). At lower frequencies, the system is actively held away from thermal equilibrium—an effect that, according to the model, results from the feedback between channels and associated motors. If this feedback is turned off, the model satisfies the fluctuation–dissipation theorem ($T_{eff} = T$) throughout the frequency range.

Nonlinear Compression and Phase Locking

When stimulated at BF($|\tilde{\chi}_0|$), the resulting phase-locked displacement of the fly's antennal receiver scaled nonlinearly with the stimulus force (Figure 4A): The ratio between displacement and stimulus amplitudes, which provides a measure of mechanical sensitivity, was constant for high and low stimulus amplitudes (linear regimes) but dropped in between (nonlinear regime, ~0.1–10 pN), leading to a ~9-fold gain in sensitivity for weak stimulation (9 ± 3, n = 6). This compressive nonlinearity was associated with increased phase locking of the receiver's displacement to the stimulus (Supplemental Data), which was complete for stimulus amplitudes >~1 pN (Figure 4B). Both the compressive nonlinearity and this phase-locking behavior were reproduced by the general fit of the model (Figures 4A and B), which, because of deviations at high forcing amplitudes, predicted a somewhat larger sensitivity gain (15 ± 10, n = 7). According to the model, the compressive nonlinearity displayed by the fly's antennal receiver results from transducer gating and the activity of adaptation motors: If the feedback between channels and motors in the model is turned off, the nonlinear compression persists because of channel gating, but the sensitivity gain drops (1.55 ± 0.66, n= 7; Figure S1C). With feedback, the relative power that the motors contribute to the receiver's vibration, $\overline{P}_A/\overline{P}_S$, is constant for stimulus forces <~1 pN but declines if forcing is increased. For high stimulus amplitudes (>~10 pN), $\overline{P}_A/\overline{P}_S$ becomes negative if internal dissipation is neglected and approaches zero if energy dissipation due to motor friction is taken into account (Figure 4C; Supplemental Data). Hence, the transduction modules actively boost the receiver's sensitivity only for weak stimuli; for strong stimuli, frictional losses of the motors exceed their power production, effectively turning the modules for transduction into energy sinks.

Transducer Gating and Nerve Response

Stimulus-evoked displacements of the fly's antennal receiver associate with compound action potentials (CAPs) in the antennal nerve. Because stimulus-correlated action potentials will only be generated when the transducer channels' open probability exceeds their resting value, we defined an excess channel open probability (Supplemental Data) and compared it with recorded CAPs. In contrast to mechanically evoked transducer currents (which are inaccessible in the fly's ear), the measurement of mechanically evoked action potentials

(and thus CAPs) necessitates that the neuronal membrane has been depolarized beyond a distinct threshold. For small stimuli, the existence of a threshold is expected to result in relatively smaller CAP amplitudes when compared to the predicted excess open probabilities. Consistent with this assumption, we observed minor deviations between model and data for small force steps (Figure 2A). On the whole, however, the excess open probabilities displayed peak amplitudes that were approximately proportional to those of the CAPs for both step-like and sinusoidal forcing (Figures 2A and 4D). Measured CAPs and predicted excess open probabilities also displayed similar temporal patterns (Figure 4E). Mechanically evoked electrical responses in the fly's antennal nerve thus share basic properties with the transducer characteristics the model predicts.

Discussion

Profiting from the experimental accessibility of the *Drosophila* hearing organ and linking measurements and theory, this study shows that transduction modules, like those proposed for vertebrate hair cells, explain the active in vivo performance of an entire ear. Our experimental data document active properties for the fly's antennal sound receiver that closely resemble those reported for the sensory hair bundles of vertebrate hair cells, including a transient nonlinear compliance in response to force steps [21, 22, 25] (Figures 2A and B), a linear response function with a negative imaginary part [16] (Figure 3A), frequency-specific cycle-by-cycle amplification of oscillatory stimuli [15] (Figures 3B and C), an effective temperature that deviates from ambient temperature [16] (Figure 3E), and a compressive nonlinearity that increases the ear's mechanical susceptibility for low-intensity sound [17] (Figure 4A). Our theoretical analysis, in turn, shows that, with some minor additions, a transduction model like that used to describe active hair-bundle mechanics [23–25] suffices to explain all these active properties of the fly's sound receiver, as well as its free fluctuations (Figure 3D), its phase-locking behavior (Figure 4B), and properties of mechanically evoked nerve responses (Figures 2A, 4D, and 4E). As judged from our analysis, the active performance of the fly's antennal receiver can be understood as the result of interactions between receiver and transducer dynamics, whereby activity emerges from alterations of the force-velocity characteristics of adaptation motors due to transducer gating. We note that although the mechanical properties of the molecular modules for auditory transduction cannot be probed more directly, the good qualitative and quantitative agreement between theory and experiments supports this interpretation; deviations between measured and predicted responses mainly occur at large forcing amplitudes, at which amplification becomes negligible and nonlinearities other than the force dependence of channel open probabilities may become important. We also note that our transducer-based model of the *Drosophila* hearing organ is minimal in that only necessary and reasonable assumptions are being made: (1) Measurements on dead and mutant flies have shown that the fly's antennal sound receiver proper behaves like a simple harmonic oscillator [29]. (2) The existence of two opposing transducer populations in the fly's auditory organ, in turn, is consistent with anatomical observations [32–34], the frequency doubling of compound nerve responses [31], and Ca^{2+}-imaging results (A. Kamikouchi, A. Fiala, and M.C. Göpfert, unpublished data). (3) Submillisecond latencies of nerve responses indicate that the displacements of the fly's antennal receiver directly gate the transducer channels [31], and adaptive shifts of the receiver's transient nonlinear compliance indicate that transducer adaptation is complete [31]. The simplest transduction model that allows for transient nonlinear compliances and complete adaptation is the conventional gating-spring model with channel, motors, and spring [21]. In principle, the motors could be replaced by dashpots that slide in response to forcing, yet such passive arrangement allows for neither force generation nor active cycle-by-cycle amplification. Active amplification requires molecular motors, and the conventional gating-spring model allows for amplification if channel open probabilities and motor activities are linked [23]. As in hair cells, this linkage may be Ca^{2+}-mediated for disrupting Ca^{2+}-permeable channels in the fly's auditory neurons alters the amplificatory gain [30].

Compared to the up to ~1000-fold amplification in the mammalian cochlea [35], the sensitivity gain provided by active amplification in the fly's ear (~10-fold) is small, resembling that reported for the oscillating hair bundles of single hair cells [17]. Unlike oscillating hair bundles, however, the fly's auditory system achieves this amplificatory gain in a quiescent state; as judged from our model, the system's operating point is located in a monostable regime close to a bistable region, which means that oscillations can arise if the motor characteristics change (Figure 4F). For this oscillatory state, our model predicts considerable sensitivity gains (>1000-fold; Figure S1), consistent with the receiver oscillations associating with high amplificatory gains (of up to ~100-fold) that have been observed after pharmacological [28, 29] and genetic [30] manipulations.

Linking transducer dynamics and auditory-system performance, our analysis has mechanistic and evolutionary implications. First, fly and vertebrate transducers share physical properties and seem to work in equivalent ways. Molecular parameters that can be deduced from our model and those reported for vertebrate hair cells are of the same order of magnitude, with millisecond time constants of motor adaptation (4–12 ms in flies [Table S2] versus 12–70 ms in hair cells [20, 36, 37]) and mechanical energies required to open single transduction channels (10–13 zJ in flies [Table S2] and 7–19 zJ in hair cells [21, 38]) hardly exceeding the energy of thermal noise (4 zJ). Second, by extending transducer-based power amplification from hair cells to fly ears, our analysis supports transducer-based force generation as a widespread mechanism for amplification in hearing. Additional or alternative amplificatory mechanisms, such as prestin-mediated somatic electromotility [39], may have arisen in the course of vertebrate [40, 41] and, possibly, insect [42] evolution to account for the particular energetic needs of high-frequency hearing; at least at subkilohertz frequencies, however, considerable amplification can be achieved by means of a transducer-based process alone (Figure S1). Third, our findings highlight the central role in hearing played by transducer modules, which transduce and amplify stimulus forces, seem to dictate electrical nerve responses, and boost the macroscopic performance of ears. Combining transduction and amplification in one molecular module seems elegant, especially because the essential components required for transduction and feedback-regulated adaptation suffice for amplification. Fourth, the tight linkage between transduction and amplification in the fly's auditory system suggests that proteins that are required for amplification (e.g., TRPN1 [30]) may be components of the transduction modules. Applying our model to mutant flies will help to test this idea. Once the molecules that form the transduction modules in the fly's auditory system are identified, we anticipate

our model to merge into a comprehensive molecule-to-systems description of the functional workings of an ear.

Experimental Procedures

Oregon R wild-type flies were used for the experiments two to three days after eclosion. The flies were mounted ventrum-down on top of a Teflon rod with their halteres, wings, legs, and mouthparts stabilized by wax [43]. The second antennal segment was immobilized by dental glue to prevent muscle-based antennal movements. All experiments were carried out on a vibration isolation table at room temperature (20–25°C). Stimulus forces were applied electrostatically via an external electrode positioned ~300 μm behind the antenna's arista [31]. To allow for attractive and repulsive forcing, we lifted the fly's potential to 15 V against ground via a charging electrode in the thorax [31]. Stimulus forces were deduced from the receiver's fluctuations (Supplemental Data). Displacements of the receiver were measured at the tip of the arista using a PSV-400 Laser Doppler vibrometer with an OFV-70 close-up unit (70 mm focal length) and a DD-5000 displacement decoder. Compound action potentials were recorded via an electrolytically tapered tungsten electrode inserted between the antenna and head; the charging electrode in the thorax was used as indifferent electrode. Data were sampled at a rate of 50 kHz for offline analysis. The entire experimental protocol lasted ~1 hr. During this time, the free fluctuations of the receiver were assessed at regular intervals to test for long-term changes in auditory performance. The data were used only if the fluctuations remained more or less constant.

Supplemental Data

Supplemental Data include Supplemental Experimental Procedures, one figure, and two tables and can be found with this article online at http://www.current-biology.com/cgi/content/full/18/18/1365/DC1/.

Acknowledgments

We thank Thomas Effertz for help with the measurements, Frank Jülicher for fruitful discussions, and Michael Dübbert and Oliver Hendrich for technical assistance. This research was supported by research fellowships from the Volkswagen Foundation (to B.N.) and Deafness Research UK (to J.T.A.), grants from the Volkswagen Foundation and the German BMBF National Bernstein Network for Computational Neuroscience (to M.C.G.), and a startup grant from the University of Cologne (to M.C.G.).

Received: June 25, 2008
Revised: July 31, 2008
Accepted: July 31, 2008
Published online: September 11, 2008

References

1. Gold, T. (1948). Hearing. II. The physical basis of the action of the cochlea. Proc. R. Soc. Lond. B. Biol. Sci. *135*, 492–498.
2. Hudspeth, A.J. (1989). How the ear's works work. Nature *341*, 397–404.
3. Dallos, P. (1992). The active cochlea. J. Neurosci. *12*, 4575–4585.
4. Robles, L., and Ruggero, M.A. (2001). Mechanics of the mammalian cochlea. Physiol. Rev. *81*, 1305–1352.
5. Eguiluz, V.M., Ospeck, M., Choe, Y., Hudspeth, A.J., and Magnasco, M.O. (2000). Essential nonlinearities in hearing. Phys. Rev. Lett. *84*, 5232–5235.
6. Camalet, S., Duke, T., Jülicher, F., and Prost, J. (2000). Auditory sensitivity provided by self-tuned critical oscillations of hair cells. Proc. Natl. Acad. Sci. USA *97*, 3183–3188.
7. Lukashkin, A.N., Walling, M.N., and Russell, I.J. (2007). Power amplification in the mammalian cochlea. Curr. Biol. *17*, 1340–1344.
8. Fettiplace, R., and Hackney, C.M. (2006). The sensory and motor roles of auditory hair cells. Nat. Rev. Neurosci. *7*, 19–29.
9. Davis, H. (1983). An active process in cochlear mechanics. Hear. Res. *9*, 79–90.
10. Ashmore, J., and Gale, J. (2004). The cochlear amplifier. Curr. Biol. *14*, R403–R404.
11. Chan, D.K., and Hudspeth, A.J. (2005). Ca^{2+} current-driven nonlinear amplification by the mammalian cochlea in vitro. Nat. Neurosci. *8*, 149–155.
12. Manley, G.A. (2001). Evidence for an active process and a cochlear amplifier in nonmammals. J. Neurophysiol. *86*, 541–549.
13. Göpfert, M.C., and Robert, D. (2001). Active auditory mechanics in mosquitoes. Proc. Biol. Sci. *268*, 333–339.
14. He, D.Z.Z., Jia, S., and Dallos, P. (2004). Mechanoelectrical transduction of adult outer hair cells studied in a gerbil hemicochlea. Nature *429*, 766–770.
15. Martin, P., and Hudspeth, A.J. (1999). Active hair-bundle movements can amplify a hair cell's response to oscillatory mechanical stimuli. Proc. Natl. Acad. Sci. USA *96*, 14306–14311.
16. Martin, P., Hudspeth, A.J., and Jülicher, F. (2001). Comparison of a hair bundle's spontaneous oscillations with its response to mechanical stimulation reveals the underlying active process. Proc. Natl. Acad. Sci. USA *98*, 14380–14385.
17. Martin, P., and Hudspeth, A.J. (2001). Compressive nonlinearity in the hair bundle's active response to mechanical stimulation. Proc. Natl. Acad. Sci. USA *98*, 14386–14391.
18. Martin, P., Bozovic, D., Choe, Y., and Hudspeth, A.J. (2003). Spontaneous oscillation by hair bundles of the bullfrog's sacculus. J. Neurosci. *23*, 4533–4548.
19. Corey, D.P., and Hudspeth, A.J. (1983). Kinetics of the receptor current in bullfrog saccular hair-cells. J. Neurosci. *3*, 962–976.
20. Howard, J., and Hudspeth, A.J. (1987). Mechanical relaxation of the hair bundle mediates adaptation in mechanoelectrical transduction by the bullfrogs saccular hair cell. Proc. Natl. Acad. Sci. USA *84*, 3064–3068.
21. Howard, J., and Hudspeth, A.J. (1988). Compliance of the hair bundle associated with gating of mechanoelectrical transduction channels in the bullfrog's saccular hair cell. Neuron *1*, 189–199.
22. Hudspeth, A.J., Choe, Y., Mehta, A.D., and Martin, P. (2000). Putting ion channels to work: Mechanoelectrical transduction, adaptation, and amplification by hair cells. Proc. Natl. Acad. Sci. USA *97*, 11765–11772.
23. Nadrowski, B., Martin, P., and Jülicher, F. (2004). Active hair-bundle motility harnesses noise to operate near an optimum of mechanosensitivity. Proc. Natl. Acad. Sci. USA *101*, 12195–12200.
24. Clausznitzer, D., Lindner, B., Jülicher, F., and Martin, P. (2008). Two-state approach to stochastic hair bundle dynamics. Phys. Rev. E Stat. Nonlin. Soft Matter Phys. *77*, 041901–041913.
25. Tinevez, J.-Y., Jülicher, F., and Martin, P. (2007). Unifying the various incarnations of active hair-bundle motility by the vertebrate hair cell. Biophys. J. *93*, 4053–4067.
26. LeMasurier, M., and Gillespie, P.G. (2005). Hair-cell mechanotransduction and cochlear amplification. Neuron *48*, 403–415.
27. Göpfert, M.C., and Robert, D. (2001). Biomechanics. Turning the key on *Drosophila* audition. Nature *411*, 908.
28. Göpfert, M.C., and Robert, D. (2003). Motion generation by *Drosophila* mechanosensory neurons. Proc. Natl. Acad. Sci. USA *100*, 5514–5519.
29. Göpfert, M.C., Humphris, A.D.L., Albert, J.T., Robert, D., and Hendrich, O. (2005). Power gain exhibited by motile mechanosensory neurons in *Drosophila* ears. Proc. Natl. Acad. Sci. USA *102*, 325–330.
30. Göpfert, M.C., Albert, J.T., Nadrowski, B., and Kamikouchi, A. (2006). Specification of auditory sensitivity by *Drosophila* TRP channels. Nat. Neurosci. *9*, 999–1000.
31. Albert, J.T., Nadrowski, B., and Göpfert, M.C. (2007). Mechanical signatures of transducer gating in the *Drosophila* ear. Curr. Biol. *17*, 1000–1006.
32. Göpfert, M.C., and Robert, D. (2002). The mechanical basis of *Drosophila* audition. J. Exp. Biol. *205*, 1199–1208.
33. Kamikouchi, A., Shimada, T., and Ito, K. (2006). Comprehensive classification of the auditory sensory projections in the brain of the fruit fly *Drosophila melanogaster*. J. Comp. Neurol. *499*, 317–356.
34. Caldwell, J.C., and Eberl, D.F. (2002). Towards a molecular understanding of *Drosophila* hearing. J. Neurobiol. *53*, 172–189.
35. Ruggero, M.A., Rich, N.C., Recio, A., Narayan, S.S., and Robles, L. (1997). Basilar-membrane responses to tones at the base of the chinchilla cochlea. J. Acoust. Soc. Am. *101*, 2151–2163.
36. Assad, J.A., and Corey, D.P. (1992). An active motor model for adaptation by vertebrate hair-cells. J. Neurosci. *12*, 3291–3309.
37. Hacohen, N., Assad, J.A., Smith, W.J., and Corey, D.P. (1989). Regulation of tension on hair-cell transduction channels - displacement and calcium dependence. J. Neurosci. *9*, 3988–3997.
38. Martin, P., Mehta, A.D., and Hudspeth, A.J. (2000). Negative hair-bundle stiffness betrays a mechanism for mechanical amplification by the hair cell. Proc. Natl. Acad. Sci. USA *97*, 12026–12031.

39. Dallos, P., and Fakler, B. (2002). Prestin, a new type of motor protein. Nat. Rev. Mol. Cell Biol. *3*, 104–111.
40. Dallos, P., Wu, X.D., Cheatham, M.A., Gao, J.G., Zheng, J., Anderson, C.T., Jia, S.P., Wang, X., Cheng, W.H.Y., Sengupta, S., et al. (2008). Prestin-based outer hair cell motility is necessary for mammalian cochlear amplification. Neuron *58*, 333–339.
41. Ashmore, J. (2008). Cochlear outer hair cell motility. Physiol. Rev. *88*, 173–210.
42. Weber, T., Göpfert, M.C., Winter, H., Zimmermann, U., Kohler, H., Meier, A., Hendrich, O., Rohbock, K., Robert, D., and Knipper, M. (2003). Expression of prestin-homologous solute carrier (slc26) in auditory organs of nonmammalian vertebrates and insects. Proc. Natl. Acad. Sci. USA *100*, 7690–7695.
43. Albert, J.T., Nadrowski, B., and Göpfert, M.C. (2006). Mechanical tracing of protein function in the *Drosophila* ear. Nat. Protoc. Published online December 3, 2006. 10.1038/nprot.2006.364.